Journal of Applied Geophysics 109 (2014) 140–149

Contents lists available at ScienceDirect

Journal of Applied Geophysics

journal homepage: www.elsevier.com/locate/jappgeo

Application of seismic velocity tomography in underground coal mines: A case study of Yima mining area, Henan, China

Wu Cai, Linming Dou *, Anye Cao *, Siyuan Gong, Zhenlei Li

State Key Laboratory of Coal Resources and Safe Mining, School of Mines, China University of Mining and Technology, Xuzhou, Jiangsu 221116, China
Key Laboratory of Deep Coal Resource Mining (Ministry of Education of China), China University of Mining and Technology, Xuzhou, Jiangsu 221116, China

ARTICLE INFO

Article history:
Received 8 April 2014
Accepted 26 July 2014
Available online 6 August 2014

Keywords:
Seismic velocity tomography
Geological structures
Stress redistribution
Rock burst
Longwall mining
Ultrasonic wave velocity

ABSTRACT

A better understanding of geological structures, stress regimes, and rock burst risks around longwall mining panels can allow for higher extraction efficiency with reduced safety concerns. In this paper, the stress change of rock mass was first examined by using ultrasonic technique into laboratory-scale rock samples. Subsequently, the active and passive seismic velocity tomograms were simultaneously applied into two study cases with field-scale. Similar characteristics can be found between the active and passive tomography results. More specifically, in the first case, a geological discontinuity was clearly indicated by a linear image in both active and passive seismic tomography results. The results of the second case suggest that seismic tomography can be used to infer stress redistribution, and assess rock burst hazard or locate high-seismicity zones. Ultimately, comparisons have been made between the results of active and passive seismic tomography. Active tomography is found to be better applied in accurately detecting stress distribution and geological structures prior to the extraction of longwall panels, while passive tomography has advantages in continuously monitoring the stress changes and assessing rock burst potential during the mining of longwall panels. This study is expected to increase the safety and efficiency of the underground mining.

1. Introduction

1.1. Problem

With the development of the mechanized longwall mining method, underground coal mining has been improved both from production and productivity point of views (Hosseini et al., 2012b, 2013). However, there are still certain risks and hidden structure defaults during mining operation that can result in a persistent safety hazard and an impediment to production. Mining activity in the Yima coal mining area (China) and elsewhere have reached the mining depths of about 1 km. The lithostatic stress at this depth is about 25 MPa and mining activity causes substantial perturbation of the ambient stress field. Abutment pressures occur along or near the boundary where material has been removed. During longwall mining, removal of coal and fracturing of adjacent material by blasting result in the transfer of stress immediately in front of the face and to the sides of the longwall panel, headgate and tailgate (Peng, 2008). In particular, the front and the side abutment pressure are important for determining the location of terminal line and the size of chain pillar, and designing the support system of the longwall panel and side entries (Peng, 2006). Moreover, concentration of stress to levels exceeding the strength of rock or structure defaults often results in catastrophic and unpredictable risks (Friedel et al., 1997), such as fallings of roof, rib, or face, and rock bursts. Herein, rock bursts are considered as a natural disaster caused by elastic strain energy emitted in a sudden, rapid, and violent way from coal or rock mass, often accompanied by an airblast or windblast and violent failures which can disrupt mine ventilation, pose a danger to miners due to flying material, and may also cause a large release of strata gas and propagate explosive dust into the air (Bräuner, 1994; Dou et al., 2012). For example, a rock burst accident (equivalent to Mw 4.1) induced by a large thrust fault caused 10 deaths and trapped 75 people at 7:18 pm local time on Nov. 3, 2011 during the headgate excavation of LW 21221 at the Yima Qianqiu coal mine, Henan Province, China.

Several methods to estimate abutment pressures, detect structure defaults, and determine rock burst hazard around the longwall mining panel have been introduced, such as drilling pulverized coal parameters (Gu et al., 2012), electromagnetic emission (He et al., 2011b; Wang et al., 2011), borehole exploration, counter stresses through bolt or pressure sensor installation (Zhang et al., 2014), and distressing through a drill. For this purpose, conventional methods are time consuming and difficult, cause disruption in production, and may generally only provide a relative state of stress in a localized area. To date, the above methods are not sufficient to meet the needs of underground mining and engineering projects. Hence, there remains the need to

* Corresponding authors at: State Key Laboratory of Coal Resources and Safe Mining, School of Mines, China University of Mining and Technology, Xuzhou, Jiangsu 221116, China. Tel./fax: +86 51683995904.
E-mail addresses: lmdou@cumt.edu.cn (L. Dou), caoanye@163.com (A. Cao).

http://dx.doi.org/10.1016/j.jappgeo.2014.07.021
0926-9851/

develop a simple, rapid, and cost-effective tool for imaging locations of high stress and mine structures under the full range of stress conditions. A better approach to performing high resolution imaging is seismic velocity tomography, which is unique because it allows for noninvasive measurement of a large region.

1.2. Approach

Seismic velocity tomography, classified as "active" and "passive" based on the type of source used (Luxbacher, 2008), has been applied in various fields including analysis of stress distribution in laboratory samples (Eberhart-Phillips et al., 1989; Meglis et al., 2005; Mitra and Westman, 2009; Nur and Simmons, 1969; Westman, 2004), mapping of geologic structures and discontinuities (Peng et al., 2002; Zhao et al., 2000), earthquake tomography (Pei et al., 2013; Ustaszewski et al., 2012; Zhang et al., 2013), rock burst hazard detection (Banka and Jaworski, 2010; Dou et al., 2012; Gong, 2010; He et al., 2011a; Lurka, 2008; Wang et al., 2012), and stress identification in underground mines (Friedel et al., 1995, 1997; Hosseini et al., 2012a, 2012b, 2013; Luo et al., 2009; Luxbacher et al., 2008; Scott et al., 2004; Westman et al., 1996, 2012). However, there are few examples of rock burst hazard detection using seismic velocity tomography, especially the passive seismic velocity tomography (Banka and Jaworski, 2010; Gong, 2010; Lurka, 2008). Meanwhile, few studies in a comparison of the active seismic velocity tomography with a passive source image calculated with mining-induced tremors (Maxwell and Young, 1993) can be found.

In this paper, the relationship between the ultrasonic wave velocity and the stress changes as load being applied to rock masses was first examined at the laboratory-scale. Subsequently, the active and passive seismic velocity tomography were simultaneously applied on the longwall mining panels to illustrate the geological discontinuity, stress redistribution, and rock burst hazard at the Yima Yuejin coal mine, Henan Province, China. Ultimately, comparisons have been made between the results of active and passive seismic tomography to help us better select the right approach for our project in underground coal mines.

2. Failure in rock masses

Rupture events are observed at scales ranging from laboratory samples to the Earth's crust, including rock failures in laboratory tests and field experiments, landslides, mining-induced seismicity, and crustal earthquakes (Amitrano, 2012). Numerous researchers have verified that rocks under stress can emit the acoustic waves in the laboratory and microseismic events in mines (Filimonov et al., 2005; Hardy, 2003; Iannacchione et al., 2004). Namely, acoustic emissions of rocks observed in the laboratory can be considered as a small-scale model of the seismicity of the Earth's crust (Scholz, 1968). In tomography, ultrasonic waves are used for laboratory studies while seismic waves are employed in the field studies (Mitra and Westman, 2009).

To understand how seismic velocity tomography can be applied in underground coal mines, we must first understand the relationship between the ultrasonic wave velocity and the mechanics parameters when load is applied to a rock in the laboratory, and how rock masses fail. For this purpose, cylindrical sandstone samples (taken from an underground coal mine) with a height of 100 mm and diameter of 50 mm were tested uniaxially in the laboratory and the parameters including axial strain, circumferential strain, axial stress, and ultrasonic wave velocity were monitored. Moreover, the Young's modulus, the compressive strength, and the dilatant strain were calculated with the above monitoring data. Fig. 1 displays the test system before the sample being loaded. There are two built-in ultrasonic sensors which function as receiver and transmitter in the upper and lower plates, respectively. At certain load intervals (i.e., 3 s), the data for the propagation velocities of acoustic waves through the sample were acquired along with the

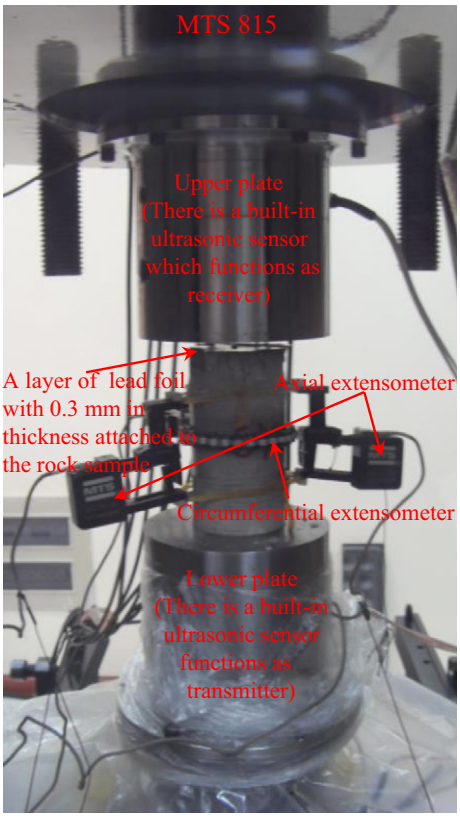

Fig. 1. Cylindrical sandstone sample with ultrasonic sensors and strain extensometers ready for testing.
Gong (2010).

sample loaded. Meanwhile, one circumferential and two axial extensometers were used for acquiring the data of the circumferential and the axial strain. It should be noted that a layer of lead foil with a 0.3 mm thickness was attached to the upper and lower surfaces of the sample, respectively.

The curves created from the monitoring results of a typical sandstone rock sample test can be found in Fig. 2. There are five stages: (1) OA stage: closure of microcracks, (2) AB stage: linear elastic deformation, (3) BC stage: stable microcrack growth, (4) CD stage: unstable microcrack propagation, (5) DE stage: macrocraking by joining of microcracks, ultimately including sliding on macrocracks. During stage one, the indenter settles into place, closing any microcracks and pore space. As this process continues, the loading reaches stage two where the rock begins to deform, which is referred to as linear elastic stage.

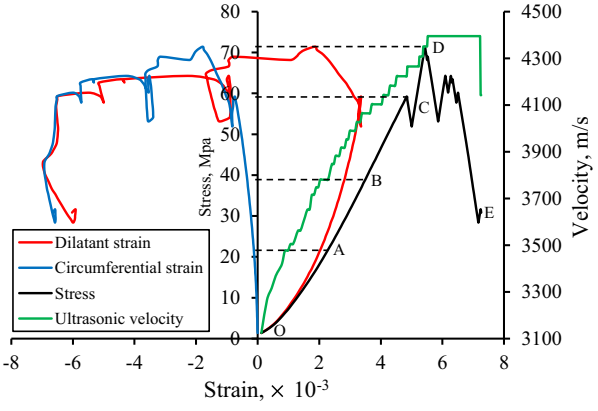

Fig. 2. Monitoring results for uniaxial compression test on a typical cylindrical sandstone sample.

During the two stages mentioned above, an exponential increase in the P-wave velocity can be found. During stage three, the new microcracks begin to grow steadily. At stage four, the density of the cracks increases, ultimately inducing failure of the rock sample. During these two stages, the P-wave velocity begins to taper off to a linear increase. Finally, just after the peak stress at point D, the microcracks coalesce into macrocracks, which may be the reason causing a linear decrease in the velocity.

The above results in the laboratory can be extended to the underground mine fields, i.e., high seismic velocity may be expected as the stress builds up prior to failure while the low velocity might be expected due to the roof cracks, gob, and structure defaults such as fault, fractured or broken zone, joint zone, and hidden voids.

3. Tomography

Tomography was first described by J. Radon (1917) who theorized that the interior of a body could be imaged by analyzing energy which passed from one boundary to another. It requires dividing the body into grid cells called pixels in two-dimensional situation, or cubes called voxels in the three-dimensional situation to estimate the characteristics of the body in all pixels or voxels (Hosseini et al., 2012b). The origins of tomography can be traced back to the discovery of the X-ray in 1895 by Wilhelm Conrad Roentgen (Stanton, 1896). Modern technology allows doctors to use X-rays to map the internal human body. Using the same key principles, scientists have extended the tomography to the geophysical field using seismic waves (Dines and Lytle, 1979). This has come to be known as seismic tomography. The P-wave is the first part of the seismic wave to arrive and generally the easiest to measure. According to the inversion parameters of the wave, seismic tomography is classified as velocity tomography and attenuation tomography (Westman, 2004; Westman et al., 1996; Zhao et al., 2000). In velocity tomography, the parameter is the inversion of velocity distribution with travel time, and attenuation tomography focuses on measuring the amplitude of seismic waves to detect the absorption property of geological media. Furthermore, the seismic velocity tomography, based on the type of source used, is classified as "active" and "passive" (Luxbacher, 2008). In underground mining, the active sources are artificially created, e.g., hammer strikes against roof and rib bolts (Friedel et al., 1995, 1997), controlled explosions (Dou et al., 2012; He et al., 2011a), and vibrations generated by the continuous coal cutter (Luo et al., 2009). In passive tomography, the mining-induced seismic events are utilized as sources (Banka and Jaworski, 2010; Glazer and Lurka, 2007; Hosseini et al., 2012a, 2012b, 2013; Lurka, 2008; Luxbacher et al., 2008; Westman et al., 2012).

Seismic velocity tomography depends on a simple relationship that the velocity along a seismic ray is the raypath distance divided by the time to travel between the source and receiver. Suppose that the raypath of the ith seismic wave is L_i with the travel time of T_i, the relationship can be described as (Hosseini et al., 2012b; Luxbacher et al., 2008; Nolet, 2008):

$$V = \frac{L}{T} \rightarrow VT = L \tag{1}$$

$$T_i = \int_{L_i} \frac{dL}{V(x,y,z)} = \int_{L_i} S(x,y,z)dL \tag{2}$$

$$T_i = \sum_{j=1}^{M} d_{ij} S_j \quad (i = 1, \cdots, N) \tag{3}$$

where T_i is the travel time, s; L_i is the raypath of the ith seismic wave; $V(x,y,z)$ is the velocity, m/s; $S(x,y,z) = 1 / V(x,y,z)$ is the slowness, s/m; d_{ij} is the distance of the ith seismic wave ray crossing the jth grid; N is the total number of rays; and M is the number of voxels.

Eq. (3) can also be expressed in matrix form as:

$$T = DS \rightarrow S = D^{-1}T \tag{4}$$

where T is the column vector of travel times ($N \times 1$); S is the column vector of slowness values ($M \times 1$); D is the matrix of ray distances ($N \times M$).

The matrix inversion methods are effective, but require considerable computational power for large datasets. Usually, the inverse problem is either underdetermined (more voxels than rays), or overdetermined (more rays than voxels) (Luxbacher et al., 2008). The most effective way to solve this problem is through the iterative process. Currently, the most referenced iterative methods are Algebraic Reconstructive Technique (ART) and Simultaneous Iterative Reconstructive Technique (SIRT) (Gilbert, 1972). SIRT is an appropriate algorithm (Hosseini et al., 2012b) and was adopted in this paper. In the process of solving, the event locations were recalculated and the slowness in each cell with regard to all the passing rays was modified once per cycle. The above steps were repeated until the residual time was less than an acceptable amount or the number of iterative reached the threshold value.

4. Case study

4.1. Site description

The Yuejin coal mine, owned and operated by Yima Coal Group Company, is located in the west of Henan Province, China. Currently, mining activity at the Yuejin coal mine occurs in LW 25110 and LW 23070, as shown in Fig. 3. The panels are fairly deep at about 970 m and 760 m underground, respectively. The fully-mechanized top coal caving method was used to retreat the panels. Up to Feb. 12, 2012, LW 23070 had been developed by the excavation of tailgate and headgate entries, and LW 25110 had been retreated for about 570 m (averaging about 1.2 m per day). Both panels were suffered by rock burst risk, making them appropriate sites for case studies for the application of seismic velocity tomography.

LW 25110 is adjacent to the gob in the north with F16 (Cai et al., 2014) thrust fault in the south and solid coal seam in the east and west. The length and the width of the panel are approximately 865 m and 191 m, respectively. The coal seam thickness ranges from 8.4 m to 13.2 m (about 11.5 m in average) with an average dip angle of 12°. The seam is overlain successively by mudstone with 18 m in thickness, coal with 1.5 m, mudstone with 4 m and glutenite with 190 m, and successively underlain by mudstone with 4 m and sandstone with 26 m. During the retreat of the longwall panel, the panel experienced mining tremors frequently and induced tens of rock bursts which caused great damage to the workface and entries, mainly in the headgate entry of the longwall.

LW 23070 is approximately 1021 m long and 210 m wide with previously mined panels to the tailgate and headgate sides, which is called the island longwall face. The coal seam ranges in thickness from 7.8 m to 10.5 m with an average dip angle of 12°. As shown in Fig. 3, there is a coalbed merging line across the panel, where the thickness of coal seam is thick in the south and thin in the north. The coal seam is overlain successively by mudstone approximately 23 m in thickness, 0.9 m coal and 105 m glutenite, underlain by mudstone with 6 m. After the tailgate and headgate entries of LW 23070 mined across the coalbed merging line, numerous seismic events with an intensity $\geq 10^5$ J began to occur. It is important to mention that eleven rock bursts that caused great damage to the entry and impeded production were induced by mining activities during the excavation of open-off cut.

Microseismic monitoring in mines allows for calculation of microseismic event source location, energy or magnitude, and source mechanisms, which can be further used as tomography to map geologic structures and discontinuities, infer the stress redistribution, and

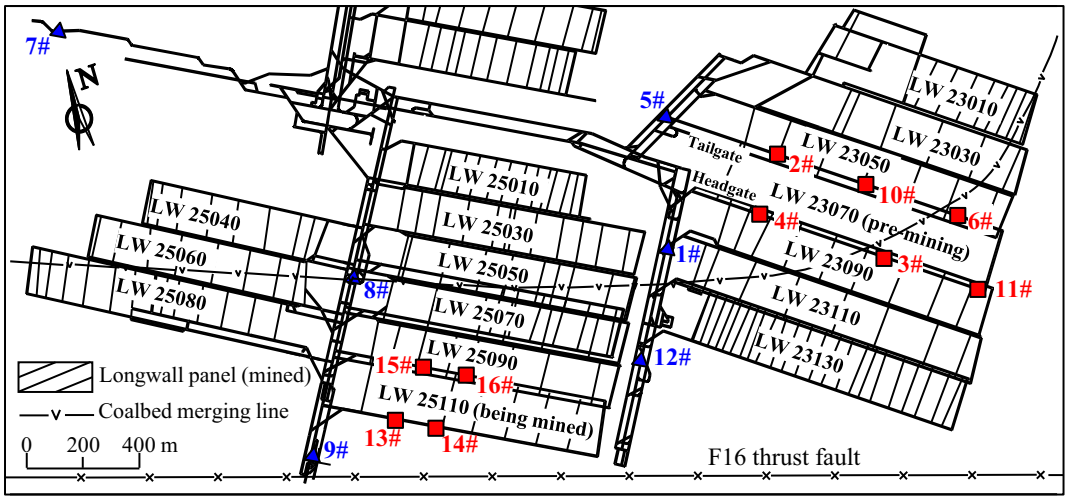

Fig. 3. Layout of the microseismic monitoring system installed in the Yima Yuejin coal mine, Henan Province, China. Squares indicate temporary stations that can be moved as the working face advances and triangles represent permanent stations.

determine rock burst hazard. Since Apr. 22, 2011, the microseismic monitoring system called "ARAMIS M/E" that was developed by the Institute of Innovative Technologies EMAG of Poland has been installed in the Yuejin coal mine. Fig. 3 displays the panel geometry and relative receiver locations, along with the face location of LW 25110 on Feb. 12, 2012, which includes six permanent stations (triangles) assembled on the decline and main entries and ten temporary stations (squares) mounted on the tailgate and headgate entries that can be moved as the working face advances.

4.2. Data acquisition

The data were collected and analyzed using *GeoPen SE2404NT* and *PASAT M* for the active seismic velocity tomography on LW 23070 and LW 25110, respectively. Seismic energy was introduced by controlled explosions along the tailgates using the blasting holes that were drilled 2 m into the coal seam and charged with 200 g of explosives. The wave data were simultaneously recorded at a quantity of single component geophones. Each geophone was screwed into a rock bolt at locations along the headgates.

Data acquisition for passive seismic velocity tomography was conducted with the microseismic monitoring system, as shown in Fig. 3, which utilizes mining-induced seismic events as the energy sources and measures the P-wave arrival time after the seismic wave passes through the rock mass. After data reduction, the data were analyzed using MINESOSTOMO program developed by Gong (2010). In order to decrease the grid model size and thereby improve the inversion efficiency, the passive seismic velocity tomography on LW 25110 was performed using the stations (8#, 9#, 12#, 13#, 14#, 15#, and 16#) and the seismic events located in the target areas. Meanwhile, the stations (1#, 2#, 3#, 4#, 5#, 6#, 10#, 11#, and 12#) and the seismic events that occurred in the target areas were used for the tomography on LW 23070. Moreover, the events recorded by more than five stations were adopted to avoid creating artificial anomaly in tomograms.

4.3. Inversion parameters

One of the most important parameters in the tomograms evaluation is typically dependent on three factors: the distribution of the velocity, the source–receiver geometry and density, and the wavelength or grid size (Hosseini et al., 2012b; Luxbacher, 2008). The tomograms in this study were generated using SIRT which must have an initial velocity value to perturb the first iteration. The initial velocity model allows the inversion and the source locations to be calculated more efficiently and accurately. The source–receiver geometry and density will also affect the calculation accuracy of the source locations, and determine how well the ray coverage of the model will be. The wavelength (or grid size) determines the resolution of seismic tomography. Some studies indicated that the theoretical resolution is about one wavelength (Williamson, 1991), although this relation is not very well-known (Soldati and Boschi, 2005; Tselentis et al., 2007).

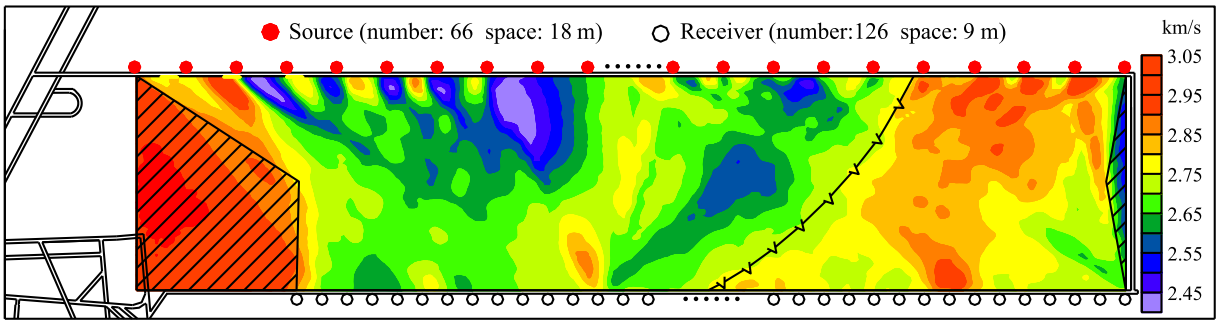

Fig. 4. Active tomographic velocity image of LW 23070 before the panel retreated. Sources are displayed in red with number of 66 and space of 18 m; receivers are displayed in black with number of 126 and space of 9 m. The dash areas indicate that no or insufficient rays traverse, thus the interpretation for these areas should be carefully made.

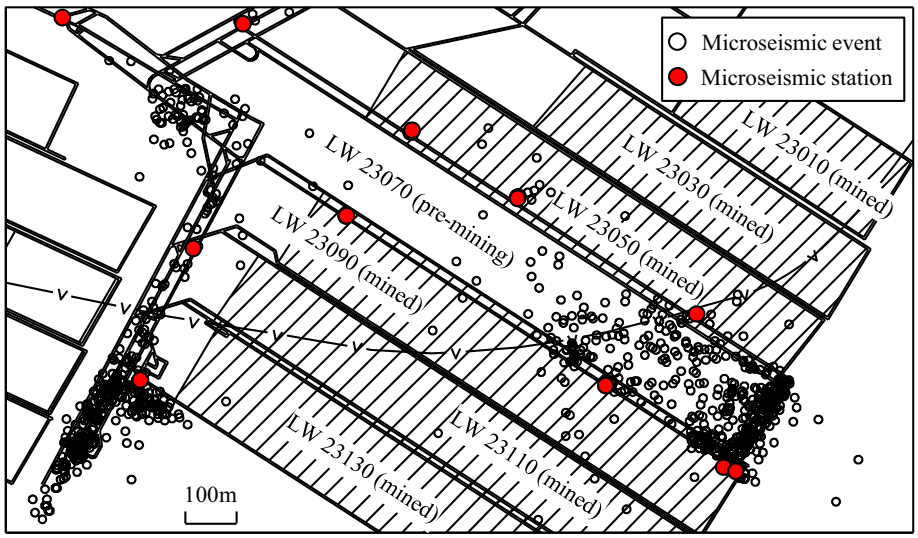

Fig. 5. Passive source–receiver configurations with mining-induced microseismic events and mounted stations around the LW 23070 panel during the period (between Nov. 1, 2011 and June 7, 2012) of the tailgate and headgate entries excavating. Sources are displayed in black and receivers are displayed in red.

In passive seismic velocity tomography, the constant velocity equal to 4 km/s was assumed in the research area to calculate the location of seismic events and perturb the first iteration. The Nyquist sampling theorem states that the sampling frequency should be at least twice the highest frequency contained in the signal. For practical engineering design, the sampling frequency is usually about five and even ten times the highest frequency. The sampling frequency of the ARAMIS M/E system used in the field is 500 Hz, thus the seismic signals with frequency between 0 and 150 Hz can be completely monitored. For a frequency of 150 Hz and a velocity of 4 km/s, the wavelength is about 26.7 m and, therefore, the ideal voxel size should be larger than 26.7 m. Moreover, the maximum epicenter location error in the study area is about 30 m, and the location error in vertical direction usually exceeds 70 m due to the fact that the seismic station geometry in underground longwall coal panels did not vary significantly in vertical direction and thereby did not constrain the events well vertically. Therefore, the voxel size of about 30 m × 30 m × 100 m was considered. To reduce the indeterminacy, a maximum velocity constraint of 6.0 km/s was imposed. In active seismic velocity tomography, a pixel size of about 7 m per side was input into the program. The average velocity of 2.45 km/s and 2.75 km/s was input as the initial velocity during the LW 25110 and LW 23070 inversions, respectively, and a maximum velocity constraint of 3.0 km/s was imposed to increase the stability of the solution.

5. Results and discussion

5.1. Detect geological discontinuity

A demonstration of active tomographic velocity imaging of LW 23070 before the panel retreated is shown in Fig. 4. There are two high-velocity zones in the image: the first is located in the vicinity of the terminal lines of LW 23050 and LW 23090, and the second is located between the open-off cut and the coalbed merging line. Moreover, a low-velocity zone appears in the center of the panel. Between the low-velocity zone and the second high-velocity zone, there exists the boundary with northeast trend, which agrees well with the coalbed merging line verified by the field observation.

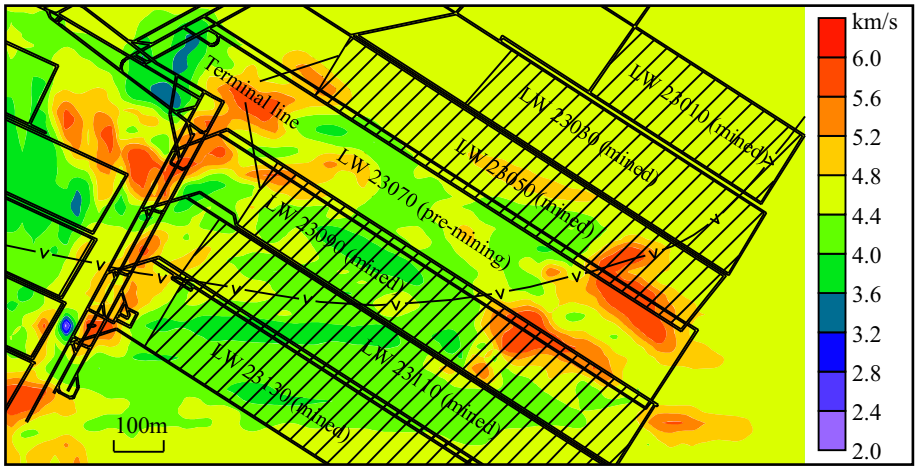

Fig. 6. Plan view of velocity tomogram at coal seam of LW 23070 during the period (between Nov. 1, 2011 and June 7, 2012) of the tailgate and headgate entries excavating.

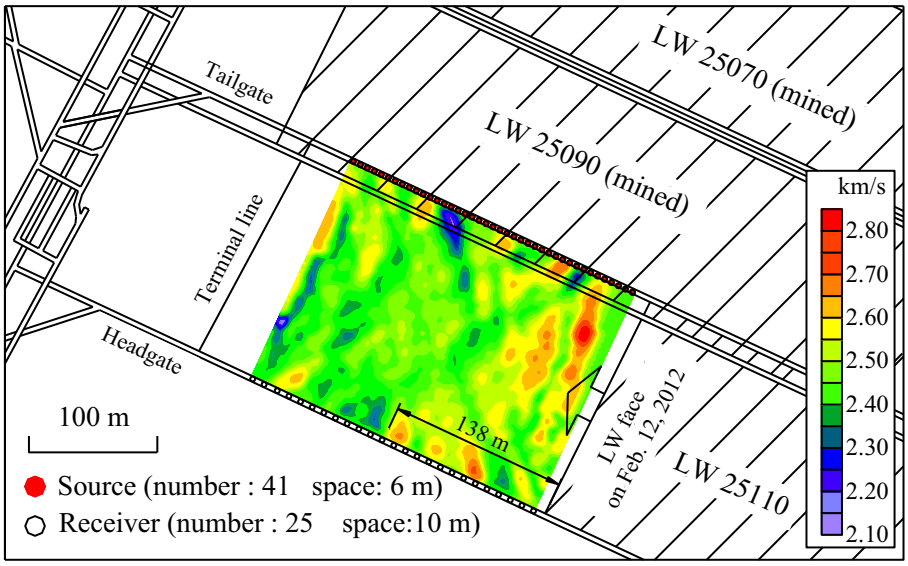

Fig. 7. Active tomographic velocity image of LW 25110 with the panel advanced on Feb. 12, 2012. Sources are displayed in red with number of 41 and space of 6 m; receivers are displayed in black with number of 25 and space of 10 m.

Meanwhile, passive tomography was conducted (Fig. 5) with mining-induced microseismic events and mounted stations around the LW 23070 during the periods (between Nov. 1, 2011 and June 7, 2012) of the tailgate and headgate entry excavations. Afterward, the plan view of velocity tomogram at coal seam of LW 23070 was obtained (see Fig. 6), which is similar in some way to the active tomographic image (see Fig. 4). As a result, the same conclusion (Zhao et al., 2000) could be obtained that seismic tomography is a powerful prospecting tool for detecting the geological discontinuity.

5.2. Estimate stress redistribution

In order to determine whether seismic tomography could be used to infer stress redistribution, the active and passive seismic velocity tomograms were simultaneously performed with the retreat of the longwall coal mining panel. Fig. 7 shows the active tomographic velocity image of LW 25110 with the panel advanced on Feb. 12, 2012, which reveals the evidence of high velocity zone just ahead of the face, corresponding to the area where front abutment pressure would be expected. Moreover, the high velocity zone is distributed about 138 m to the face along the headgate. Fig. 8 displays the passive velocity tomogram at coal seam on LW 25110 obtained from seismic events between Feb. 10 and Feb. 24, 2012, which was generated using various velocity scales and areas not traversed by seismic rays are shown in white. A high velocity zone with a scope of about 170 m can be found in front of the face. Additionally, the two tomograms displayed in Figs. 6 and 8 consistently image a relatively lower velocity zone in the gob area.

To verify that the seismic tomography could be used to infer stress redistribution, 20 groups of pressure sensors (Fig. 9) were installed in the headgate entry of LW 25110. As shown in Fig. 9, the spaces of the former ten groups and the latter eleven groups are 15 m and 25 m, respectively, and each group consists of two pressure sensors installed in 12-m-depth and 18-m-depth boreholes with a diameter of 45 mm, drilled into the coal seam. With the panel retreat, the monitoring results of the typical pressure sensors (11#, 12#, and 13#) are displayed in Fig. 10, which demonstrate that almost all of the pressure values increased significantly as the longwall face advanced in the location with approximately 130 m to the pressure sensor.

It should be mentioned that the front abutment pressure areas distribute differently using the active tomography (inference of about

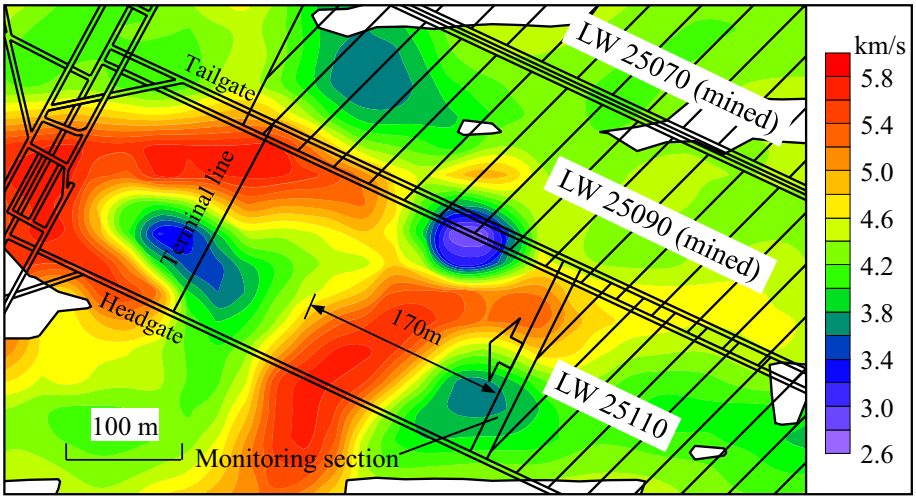

Fig. 8. Plan view of velocity tomogram at coal seam on LW 25110 obtained from seismic events between Feb. 10 and Feb. 24, 2012, and pixels not traversed by rays are shown in white. The monitoring section indicates total area mined over the inversion period.

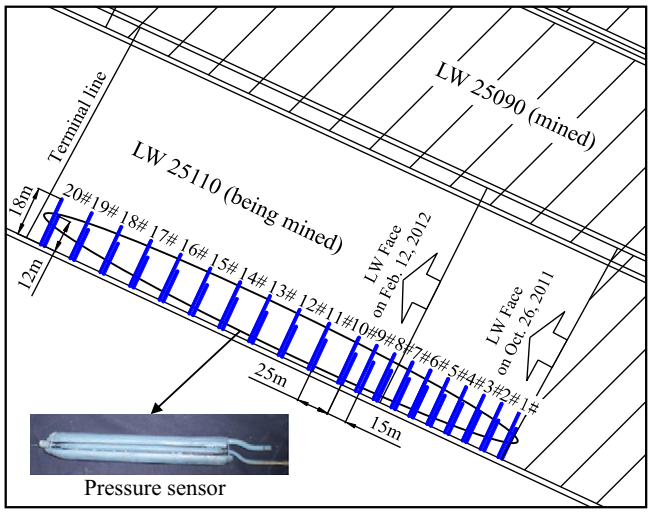

Fig. 9. Layout of 20 groups of pressure sensors installed in the headgate entry of LW 25110, at spacing of 15 m and 25 m for the former ten groups and the latter eleven groups, respectively. Each group consists of two pressure sensors installed in 12-m-depth and 18-m-depth boreholes, respectively.

138 m in Fig. 7), the passive tomography (inference of about 170 m in Fig. 8), and the pressure sensors (inference of about 130 m in Fig. 10), possibly for two reasons. The different resolution is most likely to the first reason, such as Fig. 7 (a pixel size of about 7 m per side), Fig. 8 (a pixel size of about 30 m per side in plan view), and Fig. 10 (the panel retreated for about 1.2 m in average per day). Therefore, the results should be a certain value in the intervals of 131 m to 138 m (Fig. 7), 140 m to 170 m (Fig. 8), and 130 m to 131.2 m (Fig. 10), respectively. Another reason may be as Peng (2008) stated that the stress in the surrounding rock mass of an underground mining area mostly depends on both the strength properties and the structural conditions of the rock mass which, however, are very different due to the heterogeneity of coal or rock. Especially in the passive tomographic image (Fig. 8), the longwall face advanced for about 16.2 m during the inversion period. In this period, the P-wave velocity should not be considered as invariable as the media around the longwall mining panel have surely changed.

The abovementioned results allow us to conclude that the seismic tomography can be used to infer the stress redistribution, the front abutment pressure area in this study distributed about 131 m distance in front of the face, and the resolution of the passive tomography is less than the active.

5.3. Determine rock burst hazard

During the headgate and tailgate entries of LW 23070 mining through the high velocity zones displayed in Figs. 4 and 6, the mine was experiencing roof problems, seismic tremors and even rock bursts. In particular, numerous seismic events began to occur after the entries were excavated through the coalbed merging line (Fig. 5). Furthermore, eleven rock bursts that caused great damage to the entry and impeded production occurred during the excavation of open-off cut. There is the intriguing possibility that the high velocities here may be related to the high stress zone. Moreover, a low velocity zone appears in the center of the panel, which is likely a representation of low stress concentration. Unfortunately, as explained in the tomograms (Figs. 4 and 6), no or inadequate rays are shown in the area of the open-off cut. A cluster of events would be expected, for the passive tomography (Fig. 6), which is most likely due to unconstrained event in the vertical direction. It is expected that the resolution of the active velocity image (Fig. 4) could be significantly improved if we designed some controlled explosions deployed along the open-cut off.

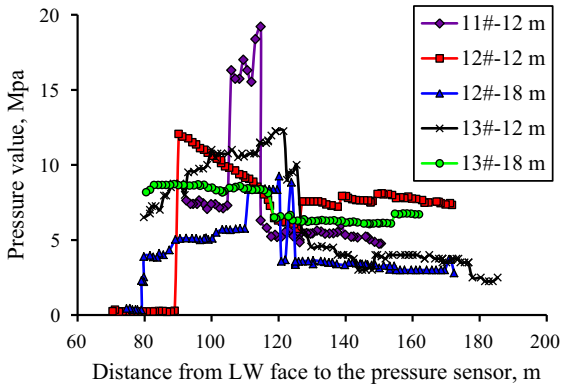

Fig. 10. Monitoring results of the typical pressure sensors (11#, 12#, and 13#) with the panel of LW 25110 retreat.

Seismic events which occurred between Feb. 25 and Mar. 25, 2012 displayed in Fig. 11, integrated with the tomograms displayed in Figs. 7 and 8, allow us to recognize that almost all of the seismic events occurred in high velocity zones. Along with the passive seismic velocity tomography to be used as a regular monitoring tool to determine the rock burst hazard or locate high seismic activity zones, tomograms were generated for every month of the study, and a good correlation between the high velocity anomalies and the high seismic activities was confirmed. One of these tomograms was conducted with mining-induced microseismic events and mounted stations around LW 25110 during the period between May 8 and June 7, 2012, as presented in Fig. 12. After the parameters were determined and the data output from MINESOSTOMO, the three-dimensional images of wave velocity were created and sliced at approximately coal seam level (Fig. 13). The symbols in Fig. 13 show positions of seismic events that occurred between June 8 and June 30, 2012. The same conclusion that almost all of the seismic events occurred in high velocity zone could be obtained. Especially in the high velocity zone near the terminal line of LW 25090, there occurred an unique strong seismic event with an intensity $\geq 10^5$ J.

5.4. Comparisons between active and passive tomography

In the field studies described above, it was stated that both the active and passive seismic velocity tomography can be used to detect geological discontinuity, estimate stress redistribution, and determine rock burst hazard, and many of the same features were evident between the active and passive tomograms.

In active seismic velocity tomography, sources of seismic waves generated by controlled explosions allow for consistent and predictable seismic raypath distribution, which can result in relatively high

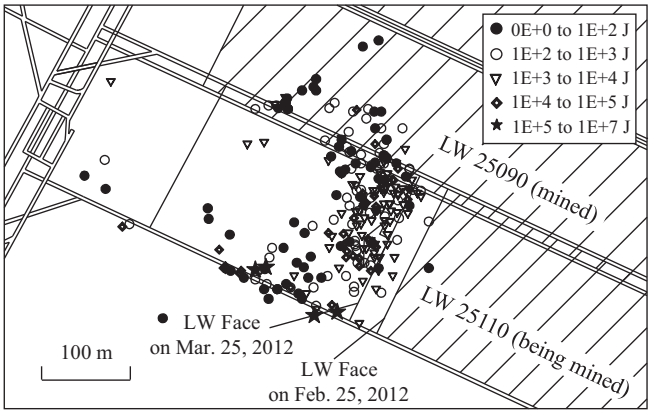

Fig. 11. Plan view of seismic events which occurred between Feb. 25 and Mar. 25, 2012.

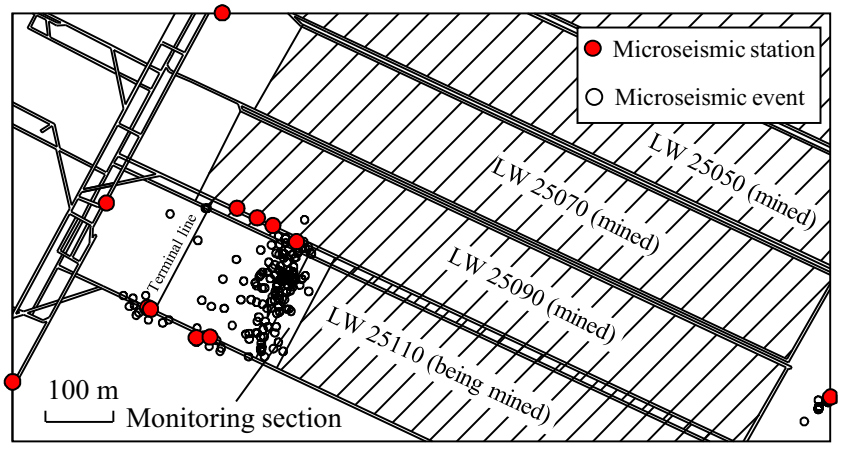

Fig. 12. Passive source–receiver configurations with mining-induced microseismic events and mounted stations around the LW 25110 during the period between May 8 and June 7, 2012. The monitoring section indicates the total area mined over the inversion period. Sources are displayed in black and receivers are displayed in red.

resolution in tomography images compared to the passive tomography. However, since the active sources usually require the presence of a person to initiate the source and record the time and location, they cause disruption in production, impose additional costs, and generally are not feasible for long term monitoring. Another practical limitation of active tomography is that the inversion area usually does not exceed the longwall panel (Figs. 4 and 7) and the information is just obtained from close vicinity of the coal seam.

Passive seismic velocity tomography, which utilizes mining-induced microseismic events, allows for monitoring over large areas where the events take place (Figs. 6 and 8), such as an entire mine, or active panel in a mine. On the other hand, since the passive sources are part of the mining operations, there is no disruption to production and costly controlled explosions are not necessary. Another advantage to routinely using these sources is that a person does not need to be physically present to initiate them, and they are practical for long term and remote monitoring, and near real time imaging of a rock mass. However, the inaccuracy in the location of the source, the high scattering, and the insufficient or irregular ray coverage are the most important shortcomings in passive tomography imaging. It results in low resolution for tomography images.

The abovementioned comparisons between the results of active and passive seismic velocity tomography allow us to recognize that the active tomography is preferred to apply in accurately detecting stress distribution and geological structures in the pre-mining longwall panel, after it has been developed by the entries excavated in coal seam, as shown in Fig. 4. While passive tomography has the potential to provide an opportunity for remote and long-term monitoring at regular time intervals over large areas, this technology is a promising tool for continuously monitoring the stress changes and assessing rock burst potential during the mining of longwall panels (see Figs. 8 and 13). As a result, precautionary measures can be taken, improving safety for miners working underground and positively impacting productivity.

It is important to note that the interpretation should be carefully made for the area with low or inadequate ray density, especially in the application of passive tomography. Additionally, passive tomography would not be appropriate with relatively few mining-induced microseismic events unless a dense receiver array is implemented.

6. Conclusions

Before seismic velocity tomography can be better applied at the field-scale, the stress changes as load being applied to rock masses were examined at the laboratory-scale by using the ultrasonic technology. Based on the experimental results, we found an exponential increase in P-velocity at low pressure that tapered off to a linear increase for higher pressure prior to failure and a linear decrease after the peak stress.

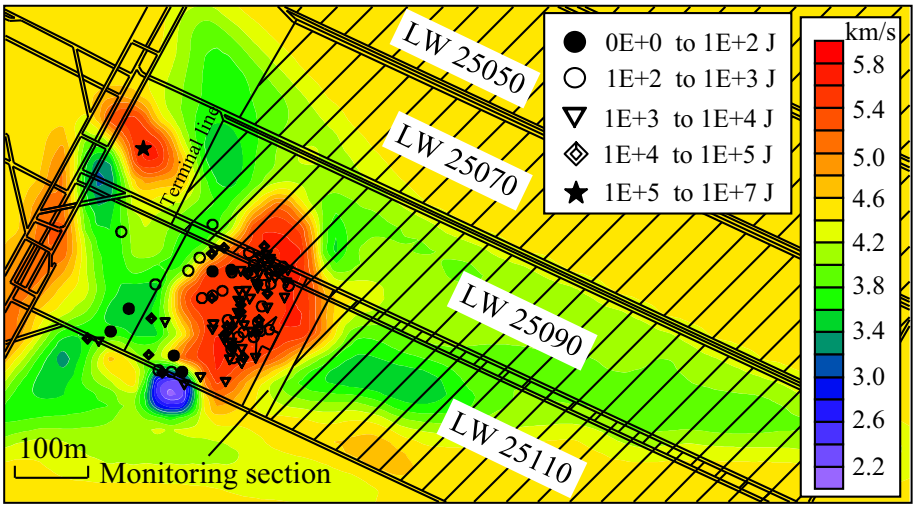

Fig. 13. Plan view of velocity tomogram at coal seam on LW 25110 obtained from seismic events between May 8 and June 7, 2012. Symbols show positions of seismic events that occurred between June 8 and June 30, 2012. The monitoring section indicates total area mined over the inversion period.

The active and passive seismic velocity tomograms were simultaneously applied on the longwall mining panels at the Yima Yuejin coal mine, Henan Province, China, and the ability of the seismic velocity tomography to illustrate geological discontinuity, stress redistribution, and rock burst hazard has been shown with two case studies and many of the same features were evident between the active and passive tomograms. The first, in the pre-mining longwall panel LW 23070, proved that the geological discontinuity was clearly indicated by a linear image of the seismic tomography, which was in good agreement with the practice. In the second case study, the tomograms of the being-mined longwall panel LW 25110 showed that the seismic tomography could be used to determine rock burst hazard or locate the high seismic activity zones, and infer the stress redistribution which was verified by the method of counter stresses through pressure sensor installation.

Although the same key principles have been used in the active and passive seismic velocity tomography, each of them has advantages and disadvantages. The active tomography is found to be better applied in accurately detecting stress distribution and geological structures prior to the extraction of longwall panels, while the passive tomography has advantages in continuously monitoring the stress changes and assessing rock burst potential during the mining of longwall panels.

In the future, the velocity tomography coupled with the attenuation tomography will assist in obtaining more accurate results. Furthermore, more traditional methods should be seized to provide any opportunity to conduct together with the seismic tomography, as this can lead to the ability to quantify the results of tomograms. With these recommendations explored, the seismic tomography in underground coal mines can be improved, contributing to a safer and more productive environment.

Acknowledgments

The Institute of Rock Pressure (Henan Dayou Energy Limited Company) and the Yuejin coal mine provided the microseismic data and the local geology. In particular, we would like to extend special thanks to Prof. Navid Hosseini and another reviewer for their useful comments and constructive suggestions, which greatly improved the quality of this manuscript. We would also like to thank Dr. Siglory for his language editing assistance.

We gratefully acknowledge the financial support for this work provided by the National Natural Science Foundation of China (51174285, 51204165), the National Basic Research Program of China (2010CB226805), the Jiangsu Natural Science Foundation (BK20130183), and the Projects supported by the Priority Academic Program Development of Jiangsu Higher Education Institution (SZBF2011-6-B35).

References

Amitrano, D., 2012. Variability in the power-law distributions of rupture events. Eur. Phys. J. Spec. Top. 205, 199–215. http://dx.doi.org/10.1140/epjst/e2012-01571-9.

Banka, P., Jaworski, A., 2010. Possibility of more precise analytical prediction of rock mass energy changes with the use of passive seismic tomography readings. Arch. Min. Sci. 55, 723–731.

Bräuner, G., 1994. Rockbursts in Coal Mines and Their Prevention. AA Balkema, Rotterdam.

Cai, W., Dou, L.M., He, J., Liu, H.S., Li, Z.L., Ding, Y.L., 2014. Mechanical genesis of Henan (China) Yima thrust nappe structure. J. Cent. South Univ. 21, 2857–2865. http://dx.doi.org/10.1007/s11771-014-2251-6.

Dines, K.A., Lytle, R.J., 1979. Computerized geophysical tomography. Proc. IEEE 67, 1065–1073. http://dx.doi.org/10.1109/PROC.1979.11390.

Dou, L., Chen, T., Gong, S., He, H., Zhang, S., 2012. Rockburst hazard determination by using computed tomography technology in deep workface. Saf. Sci. 50, 736–740. http://dx.doi.org/10.1016/j.ssci.2011.08.043.

Eberhart-Phillips, D., Han, D.-H., Zoback, M.D., 1989. Empirical relationships among seismic velocity, effective pressure, porosity, and clay content in sandstone. Geophysics 54, 82–89. http://dx.doi.org/10.1190/1.1442580.

Filimonov, Y., Lavrov, A., Shkuratnik, V., 2005. Effect of confining stress on acoustic emission in ductile rock. Strain 41, 33–35. http://dx.doi.org/10.1111/j.1475-1305.2004.00182.x.

Friedel, M.J., Jackson, M.J., Scott, D.F., Williams, T.J., Olson, M.S., 1995. 3-D tomographic imaging of anomalous conditions in a deep silver mine. J. Appl. Geophys. 34, 1–21. http://dx.doi.org/10.1016/0926-9851(95)00007-O.

Friedel, M., Scott, D., Williams, T., 1997. Temporal imaging of mine-induced stress change using seismic tomography. Eng. Geol. 46, 131–141. http://dx.doi.org/10.1016/S0013-7952(96)00107-X.

Gilbert, P., 1972. Iterative methods for the three-dimensional reconstruction of an object from projections. J. Theor. Biol. 36, 105–117. http://dx.doi.org/10.1016/0022-5193(72)90180-4.

Glazer, S., Lurka, A., 2007. Application of passive seismic tomography to cave mining operations based on experience at Palabora Mining Company, South Africa. Proceedings of The Southern African Institute of Mining and Metallurgy, 1st International Symposium on Block and Sub-level Caving, Cape Town, South Africa, pp. 369–388.

Gong, S., 2010. Research and Application of Using Mine Tremor Velocity Tomography to Forecast Rockburst Danger in Coal Mine. China University of Mining and Technology, Xuzhou, China.

Gu, S., Wang, C., Jiang, B., Tan, Y., Li, N., 2012. Field test of rock burst danger based on drilling pulverized coal parameters. Disaster Adv. 5, 237–240.

Hardy Jr., H.R., 2003. Acoustic Emission/Microseismic Activity: Volume 1: Principles, Techniques and Geotechnical Applications. Taylor & Francis.

He, H., Dou, L., Li, X., Qiao, Q., Chen, T., Gong, S., 2011a. Active velocity tomography for assessing rock burst hazards in a kilometer deep mine. Min. Sci. Technol. (China) 21, 673–676. http://dx.doi.org/10.1016/j.mstc. 2011.10.003.

He, X., Chen, W., Nie, B., Mitri, H., 2011b. Electromagnetic emission theory and its application to dynamic phenomena in coal-rock. Int. J. Rock Mech. Min. Sci. 48, 1352–1358. http://dx.doi.org/10.1016/j.ijrmms.2011.09.004.

Hosseini, N., Oraee, K., Shahriar, K., Goshtasbi, K., 2012a. Passive seismic velocity tomography and geostatistical simulation on longwall ming panel. Arch. Min. Sci. 57, 139–155. http://dx.doi.org/10.2478/v10267-012-0010-9.

Hosseini, N., Oraee, K., Shahriar, K., Goshtasbi, K., 2012b. Passive seismic velocity tomography on longwall mining panel based on simultaneous iterative reconstructive technique (SIRT). J. Cent. South Univ. 19, 2297–2306. http://dx.doi.org/10.1007/s11771-012-1275-z.

Hosseini, N., Oraee, K., Shahriar, K., Goshtasbi, K., 2013. Studying the stress redistribution around the longwall mining panel using passive seismic velocity tomography and geostatistical estimation. Arab. J. Geosci. 6, 1407–1416. http://dx.doi.org/10.1007/s12517-011-0443-z.

Iannacchione, A.T., Batchler, T., Marshall, T., 2004. Mapping hazards with microseismic technology to anticipate roof falls—a case study. Proceedings of the 23rd International Conference on Ground Control in Mining, pp. 3–5.

Luo, X., King, A., Van de Werken, M., 2009. Tomographic imaging of rock conditions ahead of mining using the shearer as a seismic source—a feasibility study. IEEE Trans. Geosci. Remote Sens. 47, 3671–3678. http://dx.doi.org/10.1109/tgrs.2009.2018445.

Lurka, A., 2008. Location of high seismic activity zones and seismic hazard assessment in Zabrze Bielszowice coal mine using passive tomography. J. China Univ. Min. Technol. 18, 177–181. http://dx.doi.org/10.1016/S1006-1266(08) 60038-3.

Luxbacher, K.D., 2008. Time-lapse Passive Seismic Velocity Tomography of Longwall Coal Mines: A Comparison of Methods. Virginia Polytechnic Institute and State University, Blacksburg, Virginia.

Luxbacher, K., Westman, E., Swanson, P., Karfakis, M., 2008. Three-dimensional time-lapse velocity tomography of an underground longwall panel. Int. J. Rock Mech. Min. Sci. 45, 478–485. http://dx.doi.org/10.1016/j.ijrmms.2007.07.015.

Maxwell, S., Young, R., 1993. A comparison between controlled source and passive source seismic velocity images. Bull. Seismol. Soc. Am. 83, 1813–1834.

Meglis, I., Chow, T., Martin, C., Young, R., 2005. Assessing in situ microcrack damage using ultrasonic velocity tomography. Int. J. Rock Mech. Min. Sci. 42, 25–34. http://dx.doi.org/10.1016/j.ijrmms.2004. 06.002.

Mitra, R., Westman, E., 2009. Investigation of the stress imaging in rock samples using numerical modeling and laboratory tomography. Int. J. Geotech. Eng. 3, 517–525.

Nolet, G., 2008. A Breviary of Seismic Tomography. Cambridge University Press, Cambridge, New York.

Nur, A., Simmons, G., 1969. Stress-induced velocity anisotropy in rock: an experimental study. J. Geophys. Res. 74, 6667–6674. http://dx.doi.org/10.1029/JB074i027 p06667.

Pei, S.P., Chen, Y.J., Feng, B.A., Gao, X., Su, J.R., 2013. High-resolution seismic velocity structure and azimuthal anisotropy around the 2010 Ms = 7.1 Yushu earthquake, Qinghai, China from 2D tomography. Tectonophysics 584, 144–151. http://dx.doi.org/10.1016/j.tecto.2012.08.020.

Peng, S.S., 2006. Longwall Mining, 2nd edition. Society for Mining, Metallurgy, and Exploration, Inc. (SME), Englewood, USA.

Peng, S.S., 2008. Coal Mine Ground Control, 3rd edition. Society for Mining, Metallurgy, and Exploration, Inc. (SME), Englewood, USA.

Peng, S., Ling, B., Liu, S., 2002. Application of seismic tomography in longwall top-coal caving face. Chin. J. Rock Mech. Eng. 21, 1786–1790.

Radon, J., 1917. Über die bestimmung von funktionen durch ihre integralwerte lange gewisser mannigfaltigkeiten. Ber. Verh. Saechs. Akad. Wiss. 69, 262–267.

Scholz, C., 1968. The frequency–magnitude relation of microfracturing in rock and its relation to earthquakes. Bull. Seismol. Soc. Am. 58, 399–415.

Scott, D.F., Williams, T.J., Tesarik, D., Denton, D.K., Knoll, S.J., Jordan, J., 2004. Geophysical Methods to Detect Stress in Underground Mines. US Department of Health and Human Services, Centers for Disease Control and Prevention, National Institute for Occupational Safety and Health, Spokane Research Laboratory.

Soldati, G., Boschi, L., 2005. The resolution of whole earth seismic tomographic models. Geophys. J. Int. 161, 143–153. http://dx.doi.org/10.1111/j.1365-246X.2005.02551.x.

Stanton, A., 1896. Wilhelm Conrad Röntgen on a new kind of rays: translation of a paper read before the Würzburg Physical and Medical Society, 1895. Nature 53, 274–276.

Tselentis, G.-A., Serpetsidaki, A., Martakis, N., Sokos, E., Paraskevopoulos, P., Kapotas, S., 2007. Local high-resolution passive seismic tomography and Kohonen neural networks—application at the Rio-Antirio Strait, central Greece. Geophysics 72, B93–B106. http://dx.doi.org/10.1190/1.2729473.

Ustaszewski, K., Wu, Y.M., Suppe, J., Huang, H.H., Chang, C.H., Carena, S., 2012. Crust–mantle boundaries in the Taiwan–Luzon arc–continent collision system determined from local earthquake tomography and 1D models: implications for the mode of subduction polarity reversal. Tectonophysics 578, 31–49. http://dx.doi.org/10.1016/j.tecto.2011.12.029.

Wang, E., He, X., Wei, J., Nie, B., Song, D., 2011. Electromagnetic emission graded warning model and its applications against coal rock dynamic collapses. Int. J. Rock Mech. Min. Sci. 48, 556–564. http://dx.doi.org/10.1016/j.ijrmms.2011.02.006.

Wang, S.W., Mao, D.B., Du, T.T., Chen, F.B., Feng, M.H., 2012. Rockburst hazard evaluation model based on seismic CT technology. J. China Coal Soc. 37, 1–6.

Westman, E.C., 2004. Use of tomography for inference of stress redistribution in rock. IEEE Trans. Ind. Appl. 40, 1413–1417. http://dx.doi.org/10.1109/TIA.2004.834133.

Westman, E., Haramy, K., Rock, A., 1996. Seismic tomography for longwall stress analysis. Rock Mech. Tools Tech. 397–403.

Westman, E., Luxbacher, K., Schafrik, S., 2012. Passive seismic tomography for three-dimensional time-lapse imaging of mining-induced rock mass changes. Lead. Edge 31, 338–345. http://dx.doi.org/10.1190/1.3694902.

Williamson, P., 1991. A guide to the limits of resolution imposed by scattering in ray tomography. Geophysics 56, 202–207. http://dx.doi.org/10.1190/1.1443032.

Zhang, F.X., Wu, Q.J., Li, Y.H., 2013. The traveltime tomography study by teleseismic P wave data in the Northeast China area. Chin. J. Geophys. 56, 2690–2700. http://dx.doi.org/10.6038/cjg20130818 (Chinese Ed.).

Zhang, N., Zhang, N., Han, C., Qian, D., Xue, F., 2014. Borehole stress monitoring analysis on advanced abutment pressure induced by longwall mining. Arab. J. Geosci. 7, 457–463. http://dx.doi.org/10.1007/s12517-013-0831-7.

Zhao, Y., Li, Q., Guo, H., Jin, H., Wang, C., 2000. Seismic attenuation tomography in frequency domain and its application to engineering. Sci. China Ser. D Earth Sci. 43, 431–438. http://dx.doi.org/10.1007/BF02959454.